20.8 A SiGe Low Noise Amplifier for 2.4/5.2/5.7GHz WLAN Applications

Po-Wei Lee, Hung-Wei Chiu, Tien-Ling Hsieh, Chih-Hsien Shen, Guo-Wei Huang[1], Shey-Shi Lu

Graduate Institute of Electronics Engineering and Department of Electrical Engineering, National Taiwan University, Taipei, Taiwan, Republic of China
[1]National Nano Device Laboratory, Hsinchu, Taiwan, Republic of China

Wireless communication has evolved into a world of multi-standards/multi-services with operating frequencies of 900MHz/1.8GHz/1.9GHz bands for GSM, 1.5GHz band for GPS and 2.4GHz/5.2GHz/5.7GHz bands for WLAN. Therefore, it is desirable to combine two or more standards in one mobile unit [1-2]. The primary challenge in designing multi-band transceivers is increasing the functionality of such communication systems while minimizing the number of additional hardware such as low noise amplifiers (LNAs). Typical design strategies [2-4] have used different LNAs for different frequency bands. However, this inevitably increases cost, power consumption and form-factor. Recently, concurrent dual-band LNAs with excellent performance have been devised, but off-chip capacitors and inductors are required [5]. In this work, an integrated SiGe LNA, which can handle the 2.4/5.2/5.7 GHz triple bands, is reported. The change of frequency bands is accomplished by switching between two different bias currents.

Figure 20.8.1 shows the schematic of our LNA. Basically, it consists of two common-emitter amplifiers. Transistor Q1 is preceded with an inductor L_B for input impedance matching. Transistor Q2 provides additional gain as well as output matching, if necessary, by using a local shunt-shunt feedback resistor R_3 around it. Note that resistive loads R_1 and R_2 instead of LC tuned loads, are used to minimize the die area.

By extending the previous work [6], it can be shown that the input impedance Z_{IN} looking into the base of a common-emitter amplifier with a parallel R_L-C_L load, as shown in Fig. 20.8.2, is equivalent to a series R_{IN}–C_{IN} network over some frequency range with the formulas indicated in Fig. 20.8.2. In our circuit, the parallel R_L-C_L load arises from the parallel combination of the resistive load of the first stage and the input impedance of the second stage. R_{IN} can be adjusted to be nearly 50 ohms by appropriate values of R_L, C_L, transconductance g_m and base-collector capacitance C_{BC}. C_{IN} is the sum of base-emitter capacitance C_{BE} and Miller capacitance C_M, and both are functions of bias current. Hence C_{IN} is varied when bias current is changed. The resonant frequency determined by C_{IN} and L_B is changed accordingly, and as a result, the resonant frequency for input matching also varies. Thus, one application band can be switched to another application band by simply switching the base current (or collector current) from one bias current to another bias current as indicated in Fig. 20.8.1. Note that the change of C_{IN} (or C_M) with bias current can be substantial because of the beneficial Miller multiplication effect. Although in this paper bias current is used to change C_{IN} (or C_M), other means can also be adopted. For example, a series combination of a capacitor and a switch can be connected between the base and collector of Q1 to achieve the same goal.

The triple band LNA shown in Fig. 20.8.1 was implemented in a standard 0.35μm SiGe BiCMOS process by the commercial foundry TSMC. The circuit parameters are: L_B = 1.39 nH, $R_1 = R_2$ = 300Ω, R_3 = 600Ω, and C_1 = 3pF. Both transistors Q_1 and Q_2 have the same emitter size of 0.3μm x 20.3μm x 2 emitter fingers. Note that the circuit (excluding the patterns for testing) occupies a very small area of 355μm x 155μm because only a small value (1.39nH) inductor L_B is used. The noise and scattering parameters were measured on wafer using an automated NP5 measurement system from ATN Microwave Inc.

The measured S parameters of the LNA at room temperature when biased with I_{B1b} current source are shown in Fig. 20.8.3. The I_{B1b} base current results in a value of collector current for Q_1 I_{C1} = 3.8mA. V_{CC} is 1.5V. The input return loss S_{11} is below –27.6dB from 2.4GHz to 2.5GHz. Power gain S_{21} is 13.8dB at 2.4GHz. S_{22} shows a very broadband matching. Note, however, for low-IF/ zero-IF applications, S_{22} does not have to be matched to 50 ohms. When I_{C1} is decreased to 3mA by switching the base current of Q1 from I_{B1b} to I_{B1a}, C_{IN} is reduced and hence the frequency band for input matching is switched to the higher frequency bands as shown in Fig. 20.8.4. Now S_{11} is below – 34.2dB from 5.1GHz to 5.4GHz and below – 21dB from 5.7GHz to 5.9GHz. S_{21} is 14.4 and 13.3dB at 5.2 and 5.7GHz, respectively. The noise performance is shown in Fig. 20.8.5. Noise figures of 3.18, 3.42 and 3.21dB are obtained at 2.4, 5.2 and 5.7GHz, respectively. The power consumptions are only 8.7 and 7.5mW for 2.4 and 5.2/5.7GHz bands, respectively.

From the experimental results, it is clear that a miniaturized fully monolithic 2.4/5.2/5.7GHz triple band LNA with low power consumption for WLAN applications is realized by a simple bias switching technique. The characteristics of the S parameters at temperatures other than room temperature are also shown in Figs. 20.8.4 and 20.8.5. From Fig. 20.8.4, it is clear that the resonant frequency of S_{11} at room temperature with I_{C1} = 3.8mA shifts to lower frequencies of 2.1 and 1.4GHz at 50 and 100°C, respectively. Nevertheless, even at 100°C S_{11} is still below –15.6dB from 2.4GHz to 2.5GHz. From Fig. 20.8.5, the resonant frequency of S_{11} at room temperature with I_{C1} = 3mA shifts to a lower frequency of 5.1GHz both at 50 and 100°C. S_{11} is still below – 34dB from 5.15GHz to 5.35GHz and below – 21dB from 5.725GHz to 5.825GHz. Noise figures at V_{CC} = 2V and room temperature were also measured and are summarized in Fig. 20.8.6. To our knowledge, the noise figure (2.73dB) achieved is a state-of-the-art result among all C-band silicon-bipolar based LNAs with on-chip matching network.

Acknowledgements
The authors thank the chip implementation center and nano device laboratory for technical support.

References
[1] T. Antes and C. Conkling, "RF Chip Set Fits Multimode Cellular/PCS Handsets," *Microwave RF*, pp. 177-186, Dec. 1996.
[2] S. Wu and B. Razavi, "A 900-MHz/1.8-GHz CMOS Receiver for Dual-Band Applications," *IEEE JSSC,* vol. 33, no. 12, pp. 2178-2185, Dec. 1998.
[3] R. Magoon, I. Koullias, L. Steigerwald, W. Domino, N. Vakillian, E. Ngompe, M. Damgaard, K. Lewis, A. Molnar, "A Triple-Band 900/1800/1900 MHz Low-Power Image-Reject Front-End for GSM," *ISSCC Dig. of Tech. Papers*, pp. 408-409, Feb. 2001.
[4] K. L. Fong, "Dual-Band High-Linearity Variable-Gain Low-Noise Amplifiers for Wireless Applications," *ISSCC Dig. of Tech. Papers*, pp. 224-225, Feb. 1999.
[5] H. Hashemi and A. Hajimiri, "Concurrent Dual-Band CMOS Low Noise Amplifiers and Receiver Architectures," *Dig. of Symposium on VLSI Circuits,* pp. 247-250, June 2001.
[6] S. S. Lu, C. C. Meng, T. W. Chen and H. C. Chen, "The Origin of the Kink Phenomenon of Transistor Scattering Parameter S22," *IEEE Trans. MTT,* vol. 49, no. 2, pp. 333-340, Feb. 2001.

 0-7803-7707-9/03/$17.00

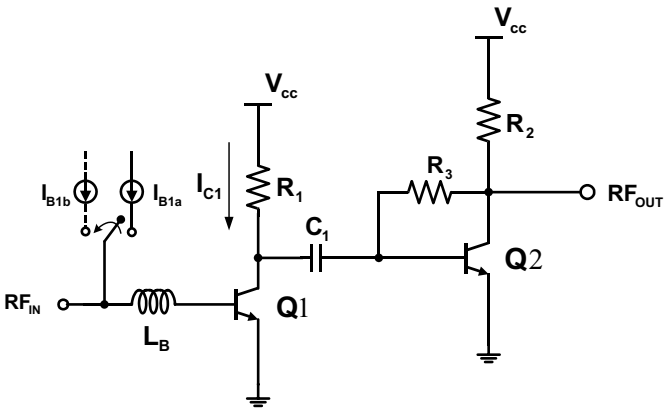

Figure 20.8.1: LNA schematic.

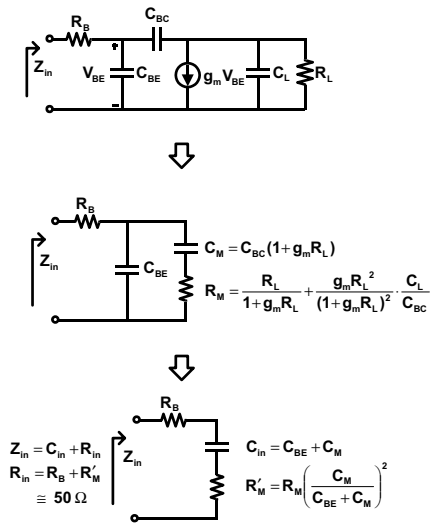

Figure 20.8.2: Method for the input matching.

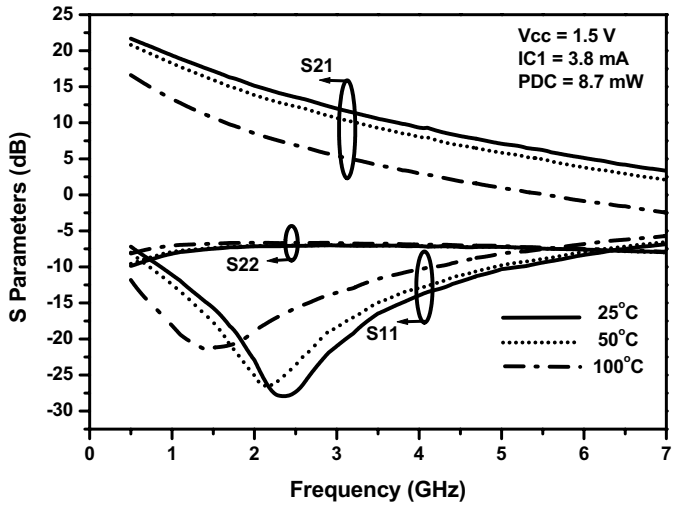

Figure 20.8.3: Measured S parameters (for 2.4GHz band).

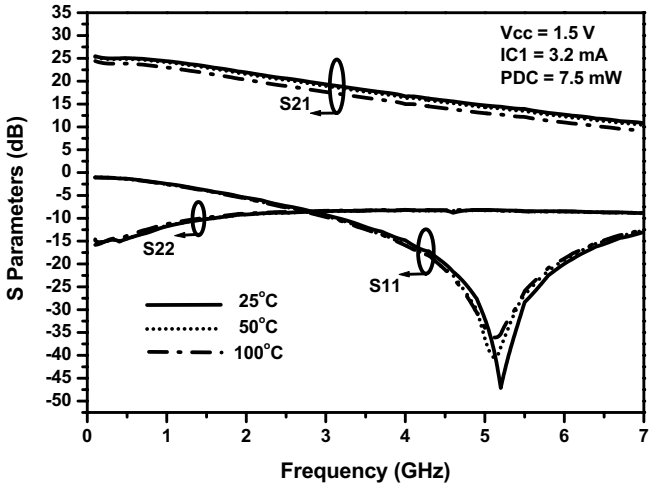

Figure 20.8.4: Measured S parameters (for 5.2/5.7GHz band).

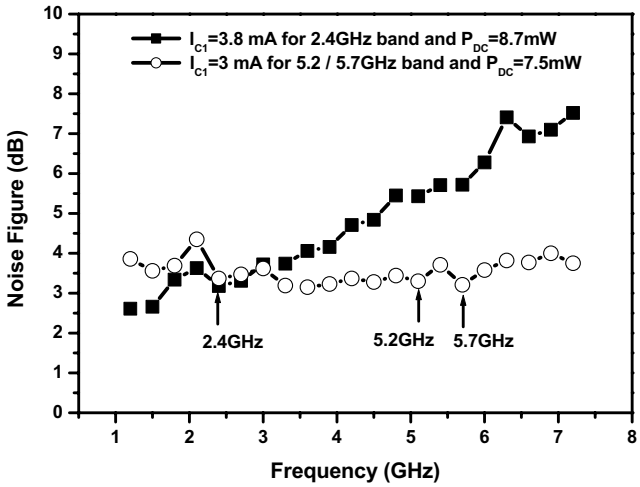

Figure 20.8.5: Measured noise figures.

V_{cc}	I_{C1}	F_c	NF	P_{DC}	Gain	S_{11}
(V)	(mA)	(GHz)	(dB)	(mW)	(dB)	(dB)
1.5	3.8	2.4	3.18	8.7	13.8	-27.6
1.5	3	5.2	3.42	7.5	14.4	-47.1
1.5	3	5.7	3.21	7.5	13.3	-24.6
2	3	5.2	2.79	13	18.4	-18
2	3	5.7	2.73	13	17.4	-17.5

Figure 20.8.6: Performance summary.

 0-7803-7707-9/03/$17.00

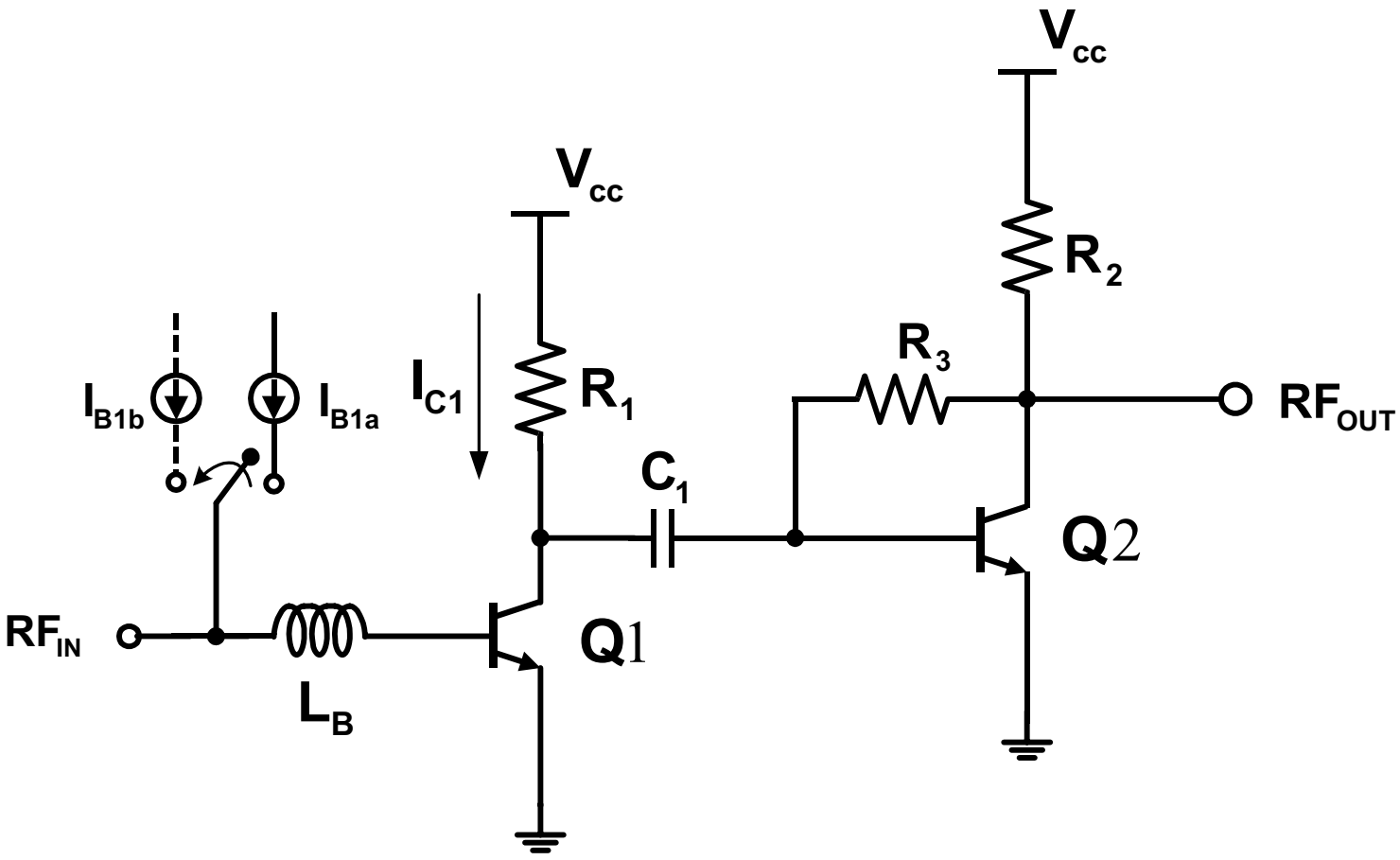

Figure 20.8.1: LNA schematic.

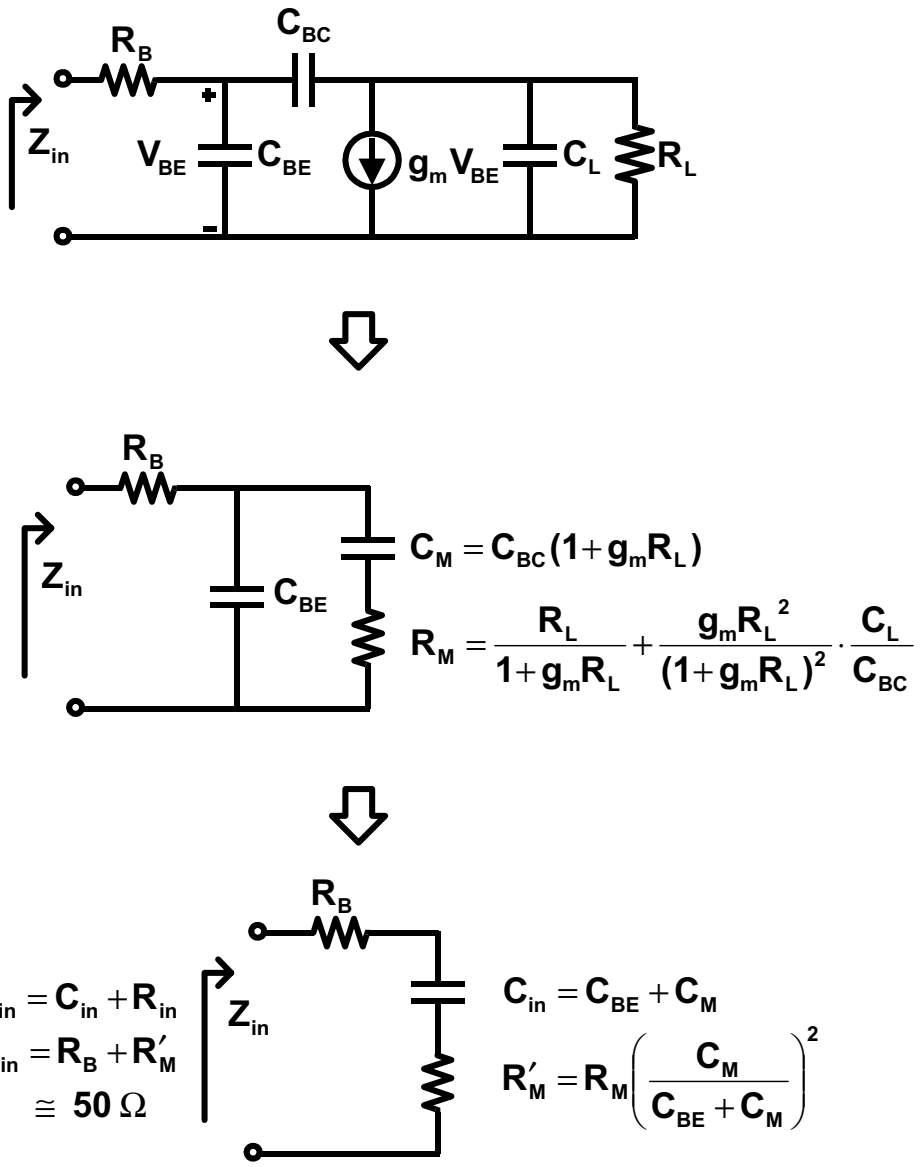

Figure 20.8.2: Method for the input matching.

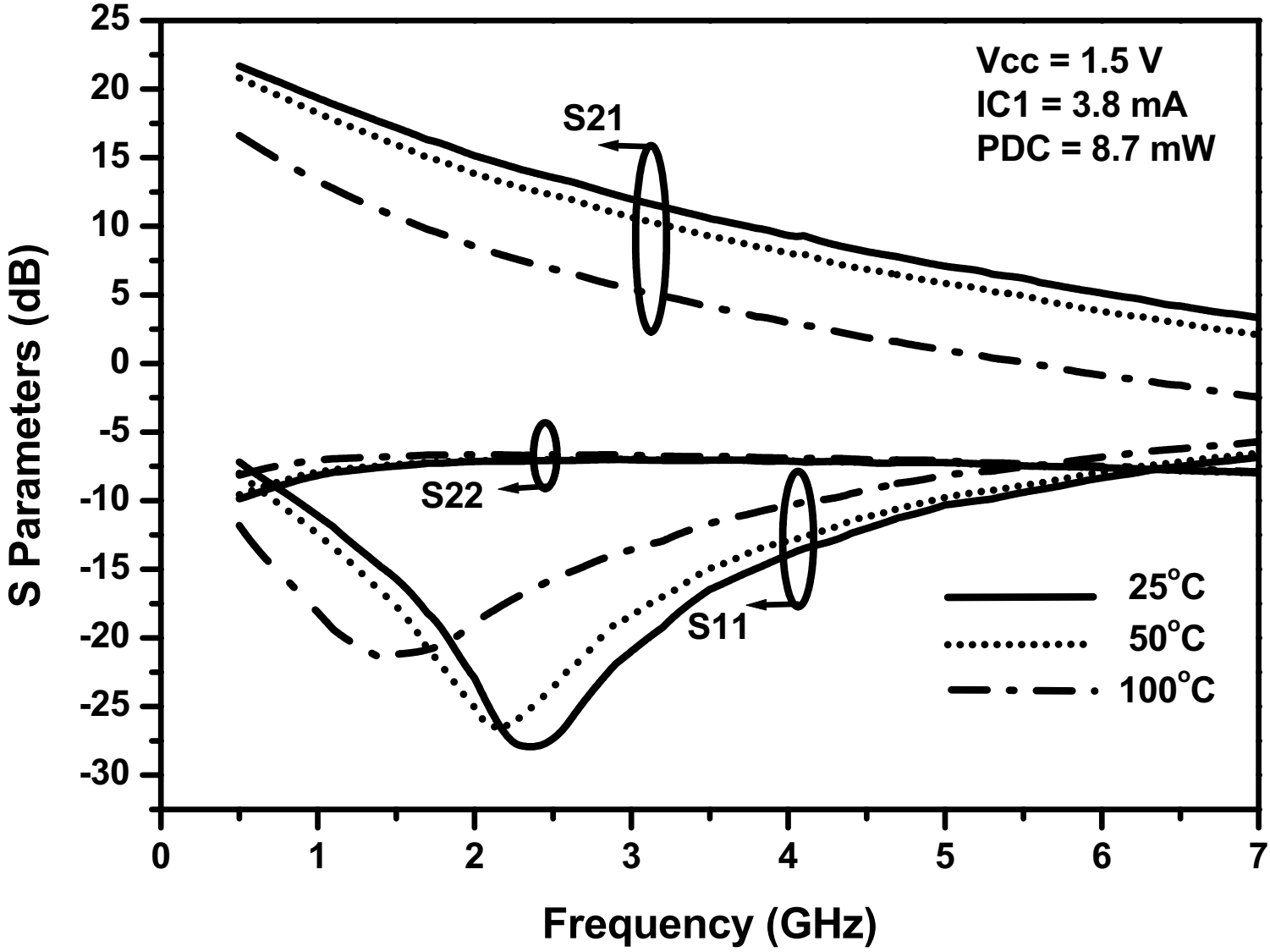

Figure 20.8.3: Measured S parameters (for 2.4GHz band).

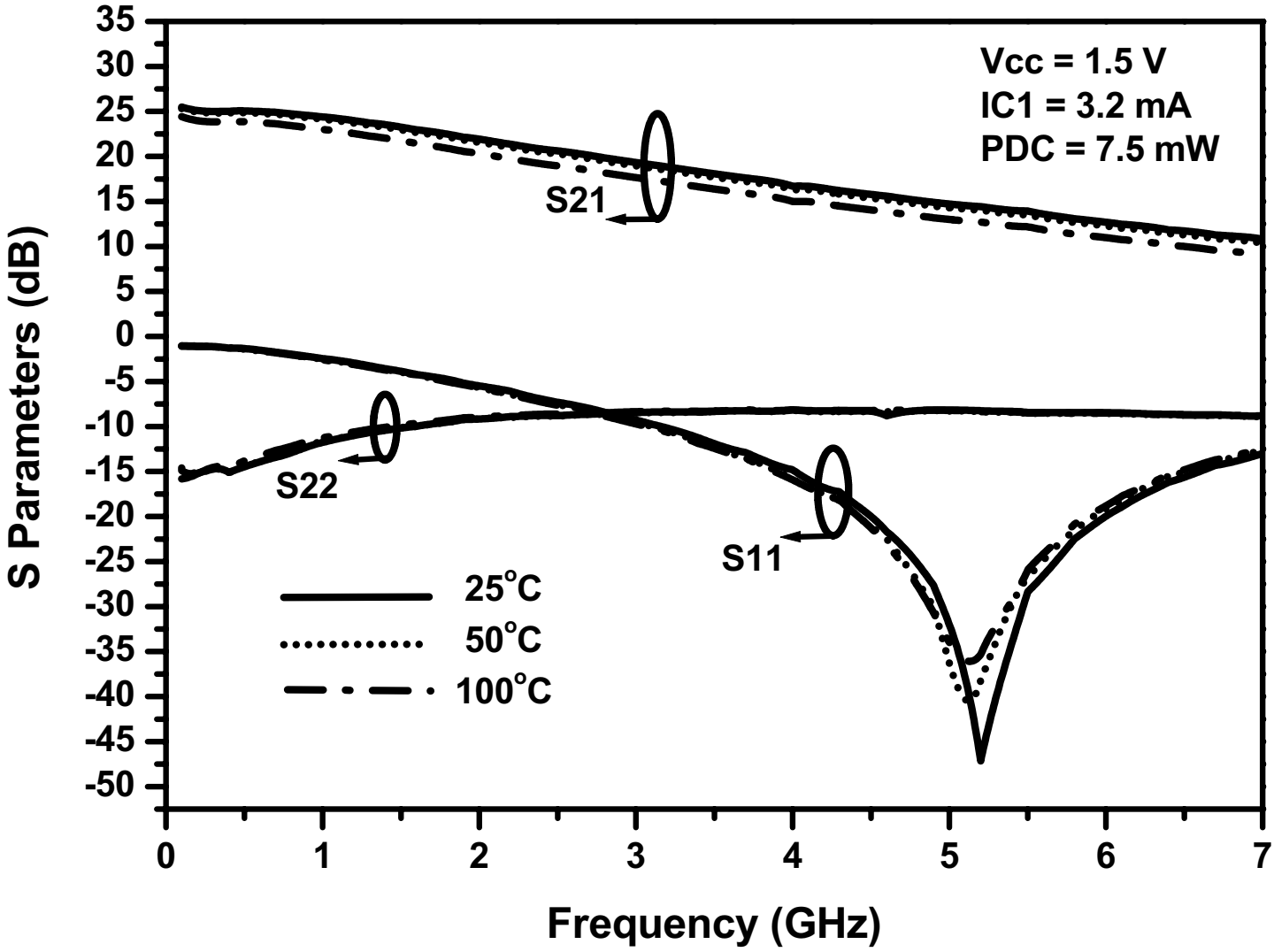

Figure 20.8.4: Measured S parameters (for 5.2/5.7GHz band).

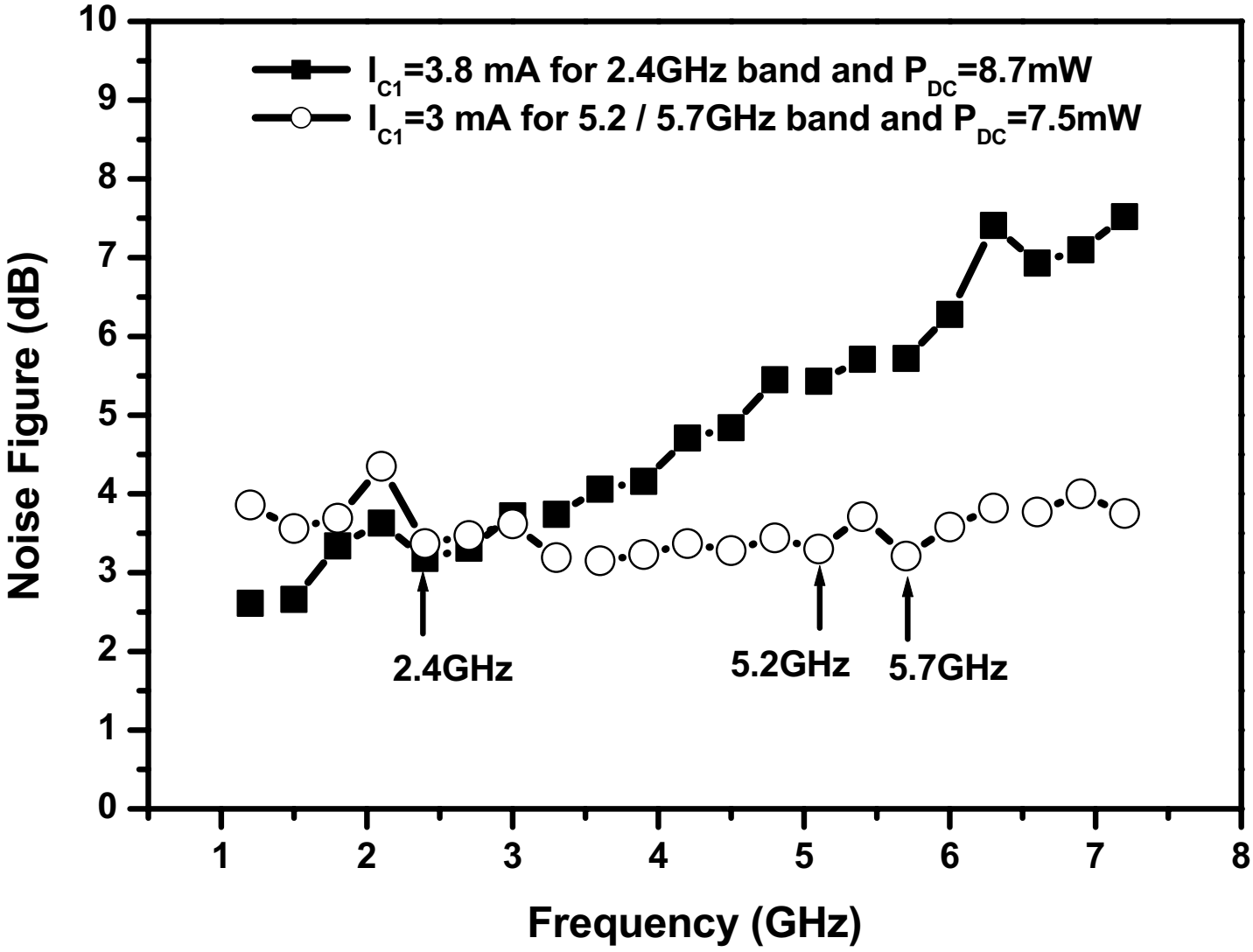

Figure 20.8.5: Measured noise figures.

V_{cc}	I_{C1}	F_c	NF	P_{DC}	Gain	S_{11}
(V)	(mA)	(GHz)	(dB)	(mW)	(dB)	(dB)
1.5	3.8	2.4	3.18	8.7	13.8	–27.6
1.5	3	5.2	3.42	7.5	14.4	–47.1
1.5	3	5.7	3.21	7.5	13.3	–24.6
2	3	5.2	2.79	13	18.4	–18
2	3	5.7	2.73	13	17.4	–17.5

Figure 20.8.6: Performance summary.